

# Limiting the dimming of distant type Ia supernovae

Linda Östman<sup>†</sup> and Edvard Mörtzell<sup>‡</sup>

<sup>†</sup> Department of Physics, Stockholm University, SE 106 91 Stockholm, Sweden

<sup>‡</sup> Department of Astronomy, Stockholm University, SE 106 91 Stockholm, Sweden

E-mail: <sup>†</sup> linda@physto.se

E-mail: <sup>‡</sup> edvard@astro.su.se

## Abstract.

Distant supernovae have been observed to be fainter than what is expected in a matter dominated universe. The most likely explanation is that the universe is dominated by an energy component with negative pressure – dark energy. However, there are several astrophysical processes that could, in principle, affect the measurements and in order to be able to take advantage of the growing supernova statistics, the control of systematic effects is crucial. We discuss two of these; extinction due to intergalactic grey dust and dimming due to photon-axion oscillations and show how their effect on supernova observations can be constrained using observed quasar colours and spectra. For a wide range of intergalactic dust models, we are able to rule out any dimming larger than 0.2 magnitudes for a type Ia supernova at  $z = 1$ . The corresponding limit for intergalactic Milky Way type dust is 0.03 mag. For the more speculative model of photons mixing with axions, we find that the effect is independent of photon energy for certain combinations of parameter values and a dimming as large as 0.6 magnitudes cannot be ruled out. These effects can have profound implications for the possibility of constraining dark energy properties using supernova observations.

## 1. Introduction

Observations of distant type Ia supernovae (SNIa) show that they are fainter than what the theory predicts for a universe described by a standard flat cold dark matter model. The most popular explanation is that the universe not only consists of luminous and dark matter, but also of large amounts of dark energy, a generic name for a homogeneously distributed energy component with negative pressure,  $p < -\rho/3$ <sup>‡</sup>. This is also verified by other cosmological probes such as the power spectra obtained from the temperature fluctuations in the cosmic microwave background [1, 2] and (on smaller scales) from large scale galaxy surveys [3, 4, 5].

Several mechanisms have been suggested in order to explain the faintness of distant SNIa without having to introduce a dark energy component. Since the existence of a large dark energy component has been independently detected by a number of

<sup>‡</sup> We do not consider any fluctuations of the dark energy component in this paper.

cosmological probes, it is unlikely that all the dimming is caused by dust or photon-axion oscillations. However, it is crucial to control all possible systematic effects in current and future SN surveys focussing on constraining the time evolution of the dark energy component.

*Supernova evolution:* Some of the apparent dimming of distant SNIa could be due to the fact that their luminosities are redshift dependent and that the SNe thus cannot be used as standard candles. This could, e.g., be caused by evolution of the SN progenitor [6, 7]. Evolutionary effects can be searched for by comparing the light curve shape and spectra of SNe at different redshifts and environments. Most studies show that the luminosity properties are rather similar [8, 9], but others have found variations indicating evolutionary effects [6, 10, 11].

*Gravitational lensing:* Since matter is inhomogeneously distributed in the universe, most line of sights to distant objects will probe a matter density significantly lower than the average density and the corresponding images will be demagnified relative to a homogeneous universe. It is generally accepted that gravitational lensing cannot be responsible for all the observed dimming of distant SNIa, however the effect may still lead to a significant bias that need to be corrected for, e.g., by using information from the magnitude distribution [12]. It has also been suggested that the large scale expansion of the universe can be affected by the inhomogeneities in the matter distribution. However, perturbative calculations show that this effect is probably negligible [13, 14].

*Photon-axion oscillations:* It has been proposed that the photon flux from SNIa may be diminished because of photons oscillating into axions in much the same way as the electron neutrino ( $\nu_e$ ) flux, produced in the sun, is diminished because of oscillations into muon neutrinos ( $\nu_\mu$ ) and tau neutrinos ( $\nu_\tau$ ). Due to differences in methods and assumptions regarding the magnetic field strengths and plasma densities, different groups have reached different conclusions about the possible magnitude and the energy dependence of the effect [15, 16, 17, 18, 19, 20].

*Intergalactic grey dust:* It has been suggested that intergalactic dust could explain the observed faintness of high redshift SNIa [21, 22]. If there is dust along the line of sight, it would extinguish some of the SN light through absorption and scattering. The intergalactic dust has to be “grey” in order not to cause a significant reddening that would have been discovered if it existed.

In this paper, we are going to discuss intergalactic dust extinction and photon-axion oscillations and show how the effects can be constrained using quasars in the first data release (DR1) from the Sloan Digital Sky Survey (SDSS). Similar studies have been performed using quasars from the SDSS early data release (EDR) for intergalactic dust [23] and for photon-axion oscillations [24]. For intergalactic dust, a maximum allowed amount of dimming of 0.2 magnitudes for SNIa at  $z = 1$  was found. In this paper we redo the analysis using the larger and higher quality data set of DR1. We also extend the range of dust models studied. In the analysis of photon-axion oscillations, there was an erroneous factor involving the photon energy in the expression for the density matrix evolution. We redo this analysis using the larger data set of DR1 with the correct

expression for the density matrix evolution.

In Section 2 we constrain the effects from photon-axion oscillations and in Section 3 we discuss limits on the intergalactic dust attenuation. In Section 4 we summarize our results.

## 2. Photon-axion oscillations

The axion is a hypothetical neutral boson with spin zero originally introduced as part of a possible solution to the strong charge-parity (CP) violation. It has also been proposed as a candidate for the missing dark matter in the universe. An axion can decay into two photons,  $a \rightarrow 2\gamma$  but also oscillate into a photon. Since they have different spin<sup>§</sup>, photons and axions can only mix in the presence of a mixing agent that preserves the quantum numbers such as angular momentum, e.g. an external transverse magnetic or electric field [25].

The photon axion interaction is described by the Lagrangian

$$\mathcal{L}_{\text{int}} = \frac{a}{M_{\text{a}}} \vec{E} \cdot \vec{B}, \quad (1)$$

where  $a$  is the axion field,  $M_{\text{a}}$  is a mass scale and  $\vec{E}$  and  $\vec{B}$  are the electrical and magnetic field, respectively. The mass scale determines the strength of the coupling.

### 2.1. Theory of the simulations

To determine the amount of dimming different scenarios of photon-axion oscillations lead to, we calculate the conversion probability for oscillations using the density matrix formalism. The evolution of a density matrix  $\rho$ , is described by [26]

$$i\hbar \frac{\partial \rho}{\partial t} = -[\rho, \mathcal{H}], \quad (2)$$

where  $\mathcal{H}$  is the Hamiltonian, which in our case is given by  $\mathcal{H} = \frac{\hbar}{2} M$ . The mixing matrix  $M$  is given by [16, 27]

$$M = \begin{pmatrix} \Delta_{\perp} & 0 & \Delta_{\text{M}} \cos \alpha \\ 0 & \Delta_{\parallel} & \Delta_{\text{M}} \sin \alpha \\ \Delta_{\text{M}} \cos \alpha & \Delta_{\text{M}} \sin \alpha & \Delta_{\text{m}} \end{pmatrix}, \quad (3)$$

where  $\alpha$  is the angle in the plane perpendicular to the propagation between a fixed polarisation vector and the projected magnetic field. The other quantities in the mixing matrix are

$$\begin{aligned} \Delta_{\perp} &= -3.6 \cdot 10^{-25} \left( \frac{\omega}{1 \text{ eV}} \right)^{-1} \left( \frac{n_{\text{e}}}{10^{-8} \text{ cm}^{-3}} \right) \text{ cm}^{-1}, \\ \Delta_{\parallel} &= \Delta_{\perp}, \\ \Delta_{\text{M}} &= 2 \cdot 10^{-26} \left( \frac{B_{0,\perp}}{10^{-9} \text{ G}} \right) \left( \frac{M_{\text{a}}}{10^{11} \text{ GeV}} \right)^{-1} \text{ cm}^{-1}, \\ \Delta_{\text{m}} &= -2.5 \cdot 10^{-28} \left( \frac{m_{\text{a}}}{10^{-16} \text{ eV}} \right)^2 \left( \frac{\omega}{1 \text{ eV}} \right)^{-1} \text{ cm}^{-1}, \end{aligned} \quad (4)$$

<sup>§</sup> The axion has spin zero while the photon has spin one.

where  $\omega$  is the photon energy,  $n_e$  is the electron density,  $B_{0,\perp}$  is the strength of the magnetic field perpendicular to the propagation of the photon,  $M_a$  is the inverse coupling between the photon and the axion, and  $m_a$  is the mass of the axion. The initial condition of the equation is

$$\rho_0 = \begin{pmatrix} \frac{1}{2} & 0 & 0 \\ 0 & \frac{1}{2} & 0 \\ 0 & 0 & 0 \end{pmatrix}, \quad (5)$$

corresponding to unpolarised light. The diagonal elements correspond to the intensities of the two polarisation states of the photon and the intensity of the axion, respectively. The system of 9 coupled (complex) differential equations is solved numerically using the SuperNova Observation Calculator (SNOC) [27]. Assuming a quasar (or a SN) at a certain redshift, the light beam from the source is followed through a large number of spherical cells. Each cell has a value for the magnetic field and the electron density. The electron density and the magnetic field strength are evolved as  $n_e \propto (1+z)^3$  and  $B \propto (1+z)^2$ . The dispersion of the field strength and the density is set to 50% of their values. We assume that the magnetic field is frozen into the plasma and subsequently given by  $B_0 \propto n_e^{2/3}$  with random direction [19]. We also test whether our simulations are in accordance with current Faraday rotation measurements. Since the magnetic domains are small compared to the total travel length and the magnetic fields have random directions, the induced Faraday rotation is too small to be used to rule out any of our investigated models. As the beam pass through the cells, the background cosmology and the wavelength of the photon are updated, as are the matrices  $\rho$  and  $M$ . In all of our simulations, we use  $[\Omega_M = 0.3, \Omega_\Lambda = 0.7, h = 0.7]$ . However, the cosmology dependence is weak.

## 2.2. Parameter dependence

The polarisation state of the photon is disregarded by rewriting  $M$  as a  $2 \times 2$  matrix,

$$M^{2D} = \begin{pmatrix} \Delta & \Delta_M \\ \Delta_M & \Delta_m \end{pmatrix}, \quad (6)$$

where  $\Delta = \Delta_\perp = \Delta_\parallel$ . After solving equation (2) analytically we find that the photon intensity,  $\rho_{11}^{2D}$ , is

$$\begin{aligned} \rho_{11}^{2D} &= 1 - \frac{\Delta_M^2}{2\Omega^2}(1 - \cos \Omega t), \\ \Omega &= \frac{1}{2}\sqrt{(\Delta - \Delta_m)^2 + 4\Delta_M^2}. \end{aligned} \quad (7)$$

Using the quantities in equation (4) we see that  $|\Delta_m| \gg |\Delta|$  when  $m_a \gg 12\sqrt{10}\sqrt{n_e/(10^{-8} \text{ cm}^{-3})}10^{-16} \text{ eV} \approx 38\sqrt{n_e/(10^{-8} \text{ cm}^{-3})}10^{-16} \text{ eV}$ . In our parameter interval for  $n_e$ ,  $B_0/M_a$ , and  $\omega$ , we then have  $|\Delta_m| \gg |\Delta_M|$  and  $\Omega \simeq \frac{1}{2}|\Delta_m| \propto m_a^2\omega^{-1}$ . For  $m_a \gg 38\sqrt{n_e/(10^{-8} \text{ cm}^{-3})}10^{-16} \text{ eV}$ , oscillations are thus suppressed as  $m_a^{-4}$  and the dimming is negligible. From now on, we assume that  $m_a \ll$

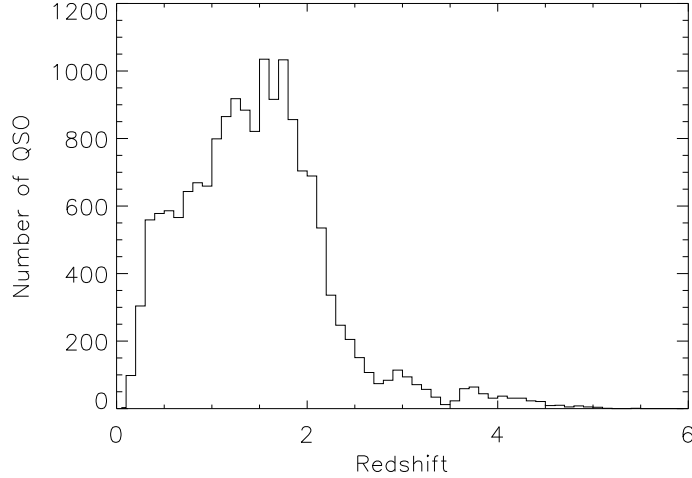


**Figure 1.** Redshift distribution of the quasars in the SDSS DR1. The redshift bins in the figure have a width of  $\Delta z = 0.1$ .

$38\sqrt{n_e/(10^{-8} \text{ cm}^{-3})}10^{-16} \text{ eV}$  where the oscillation probability is independent of the axion mass and the parameters governing the oscillation probability are the plasma density,  $n_{e0}$ , and the magnetic field divided by the inverse coupling between the photon and the axion,  $B_0/M_a^{11}$  ||, at  $z = 0$ .

In this case we have  $|\Delta_m| \ll |\Delta|$  and thus  $\Omega \simeq \frac{1}{2}\sqrt{\Delta^2 + 4\Delta_M^2}$ . For  $B\omega/(M_a n_e) \gg 9 \cdot 10^{-21} \text{ cm}^3\text{G}$ , we have  $|\Delta| \ll 2|\Delta_M|$  and  $\Omega \simeq \frac{1}{2}\Delta_M$ , i.e., the oscillations are independent of energy. This is the most important difference from the results obtained in reference [24], making it impossible to exclude any regions to the left of  $B\omega/(M_a n_e) \approx 9 \cdot 10^{-21} \text{ cm}^3\text{G}$  (see, e.g., figure 4).

### 2.3. Method

An effect of photon-axion oscillations is that a dispersion is added to the quasar spectra due to the energy dependence of the effect. By comparing the dispersion in observed quasar spectra with the dispersion in simulated quasar spectra, we can conclude if the model behind each simulation is allowed.

### 2.4. Observed quasar spectra

The spectra of 16 713 quasars are obtained from the SDSS DR1 [28]. These quasars have redshifts between  $z = 0.08$  and  $z = 5.41$  with a median redshift of  $z = 1.43$ . The redshift distribution is shown in figure 1.

The spectra are divided into redshift bins of size  $\Delta z = 0.2$  where we only consider the redshift interval  $0.1 < z < 2.9$  since we need a certain number of quasars in each

|| In the future we will use the notation  $M_a^{11} \equiv M_a/(10^{11} \text{ GeV})$ .

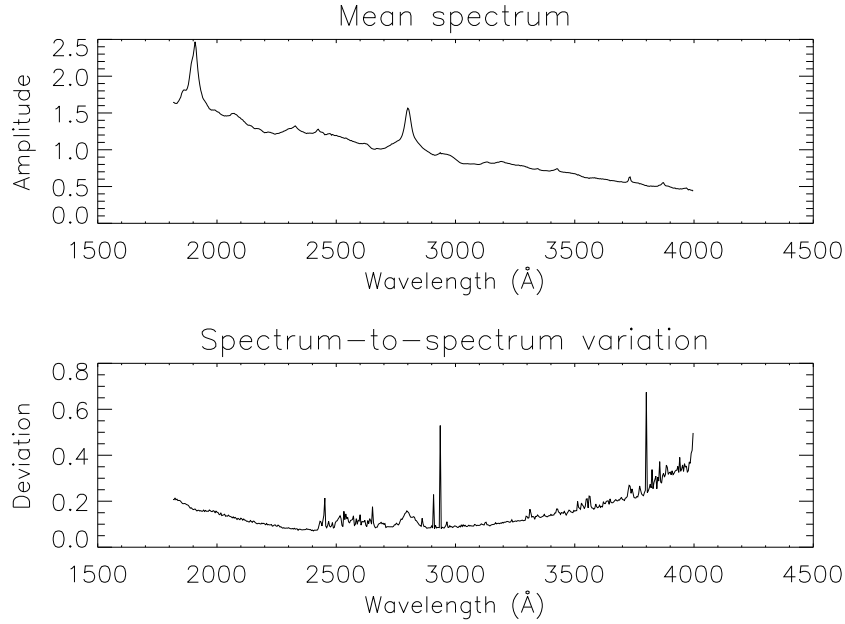


**Figure 2.** The mean rest frame spectrum and the spectrum-to-spectrum variation for the SDSS quasars with redshifts in the interval  $1.1 < z < 1.3$ .

bin to obtain acceptable statistics. In this redshift range we have 15 914 quasars.

Each spectrum is redshifted into its restframe and divided into wavelength bins of size  $4 \text{ \AA}$  and the average flux is calculated in each of these bins for the individual spectra. We calculate the mean spectrum along with the dispersion of the individual spectra from the mean spectrum in each redshift bin. All spectra more than three standard deviations from the mean are rejected in order to minimize the effect from peculiar spectra. An example of a mean spectrum and the spectrum-to-spectrum variation for a particular redshift bin is given in figure 2.

### 2.5. Simulated quasar spectra

Using SNOC, we simulate the effects of photon-axion oscillations on quasar observations for  $10^{-12} \text{ cm}^{-3} < n_{e0} < 3 \cdot 10^{-7} \text{ cm}^{-3}$  and  $10^{-11} \text{ G} < B_0/M_a^{11} < 10^{-8} \text{ G}$ , using the median quasar spectrum obtained in reference [29]. Note that the upper limit of the electron density is motivated by the WMAP measurements of the baryon density which gives a maximum allowed plasma density of  $n_e = 2.7 \cdot 10^{-7} \text{ cm}^{-3}$  [2]. In figure 3 we have plotted the normalised quasar spectrum for three different oscillation scenarios for  $z = 1$ .

For each redshift bin and set of parameter values, a large number of quasar spectra are generated and the mean spectrum and the dispersion due to the oscillations is calculated. Comparing the dispersion in the simulated and the observed quasar spectra, we are then able to constrain the values of  $n_{e0}$  and  $B_0/M_a^{11}$ . If the simulated dispersion is smaller than the observed, we cannot exclude the scenario since real quasars have an intrinsic dispersion. If the dispersion is larger for the simulated spectra, a comparison is

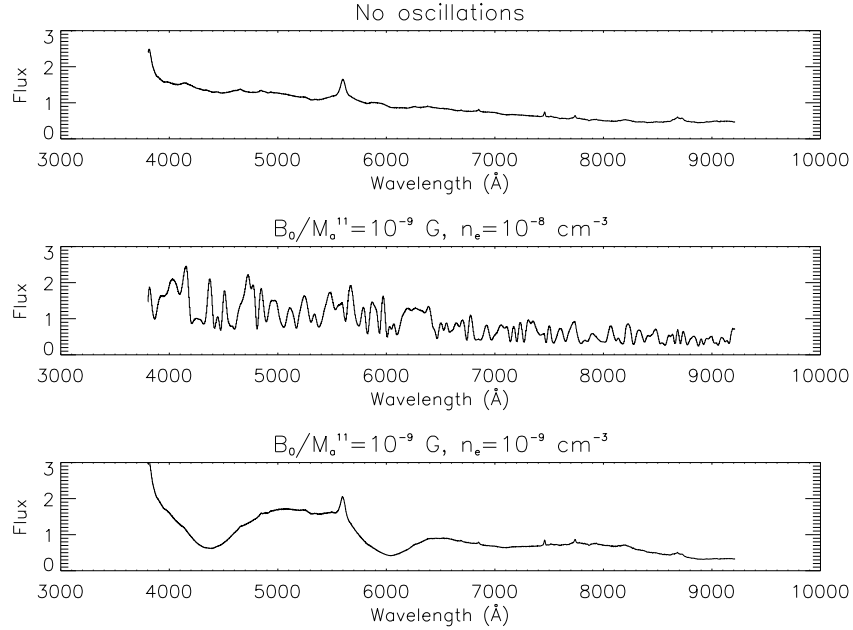


**Figure 3.** Simulated mean quasar spectra for three different scenarios when  $z = 1$ .

made between the simulated and the observed cumulative distribution of dispersions using the Kolmogorov-Smirnov test. The test gives the significance level that the distributions differ significantly for the particular redshift bin. The total significance level for a certain set of parameter values is calculated as the product of all significance levels for the different redshift bins.

For each scenario we also calculate the rest frame B-band attenuation, due to the photon-axion oscillations for a SNIa at  $z = 1$ .

## 2.6. Result

In figure 4, it is shown what values of the electron density and the magnetic field strength are allowed if there exists an axion with a mass  $m_a < 10^{-16}$  eV. The figure also contains the corresponding attenuation for a SNIa. If  $B\omega/(M_a n_e) \lesssim 9 \cdot 10^{-21} \text{ cm}^3 \text{G}$ , the dimming of SNIa at  $z = 1$  due to oscillations is less than 0.1 magnitudes. If  $B\omega/(M_a n_e) \gtrsim 9 \cdot 10^{-21} \text{ cm}^3 \text{G}$ , the oscillation probability is independent of energy and a dimming as large as 0.57 magnitudes for a SNIa at  $z = 1$  cannot be ruled out.

Note that our conclusions are conservative in the respect that we have not added any intrinsic dispersion to the simulated quasar spectra. Assuming an intrinsic dispersion of 5%, the upper limit on the dimming of SNIa at  $z = 1$  becomes less than 0.05 magnitudes when  $B\omega/(M_a n_e) \lesssim 9 \cdot 10^{-21} \text{ cm}^3 \text{G}$  (see figure 5).

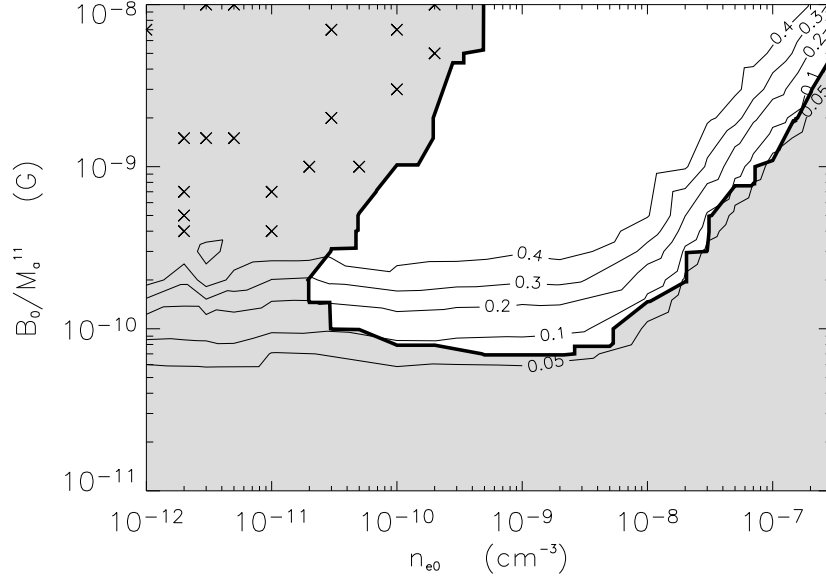


**Figure 4.** The grey region indicates the allowed parameter region at a confidence level of 95%. The lines labeled [0.4, 0.3, 0.2, 0.1, 0.05] show the B-band attenuation expressed in magnitudes for a SNIa at  $z = 1$ . The allowed simulations with a dimming larger than 0.5 magnitudes are marked with 'x'.

### 2.7. Comparison with the earlier analysis

The larger sample of the DR1 compared to the EDR leads only to minor changes in the conclusions. However, the analysis of the effects of photon-axion oscillations using EDR data in Mörtzell and Goobar [24] contained an error in the evolution of the density matrix (corresponding to equation (2) in this paper). Instead of  $2i\frac{\partial \rho}{\partial t} = [\mathcal{M}, \rho]$ , they used  $2\omega i\frac{\partial \rho}{\partial t} = [\mathcal{M}, \rho]$ . Disregarding the polarisation state of the photons (see Section 2.2), the photon intensity,  $\rho_{11}^{2D}$ , would then be given by¶

$$\begin{aligned}\rho_{11}^{2D} &= 1 - \frac{\Delta_M^2}{2\omega^2\Omega^2}(1 - \cos \Omega t), \\ \Omega &= \frac{1}{2\omega} \sqrt{(\Delta - \Delta_m)^2 + 4\Delta_M^2}.\end{aligned}\tag{8}$$

Because of the  $\omega$  in the denominator of the expression for  $\Omega$ , the oscillation probability never became independent of wavelength. Therefore, the upper left region of the plot was possible to exclude.

### 2.8. Dimming evolution

If the attenuation caused by photon-axion oscillations is large both at low and high redshifts, this cannot explain the faintness of distant SNe, even though it is still possible

¶ The corresponding equation in reference [24] had also a factor of two wrong due to a misprint. This factor was not used in the calculations.



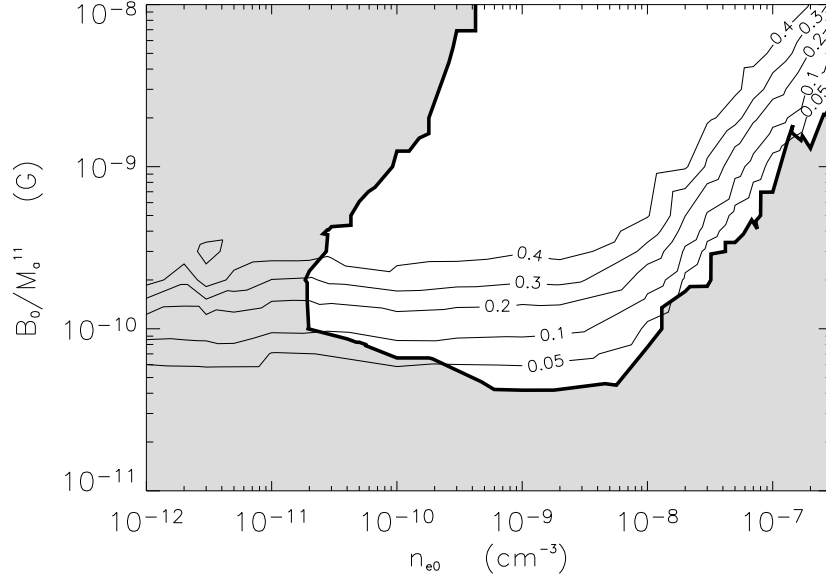


**Figure 5.** The grey region indicates the allowed parameter region at a confidence level of 95% when an intrinsic dispersion of 5% has been added to the dispersion of the simulated spectra. The thin lines show the B-band attenuation expressed in magnitudes for a SNIa at  $z = 1$ .

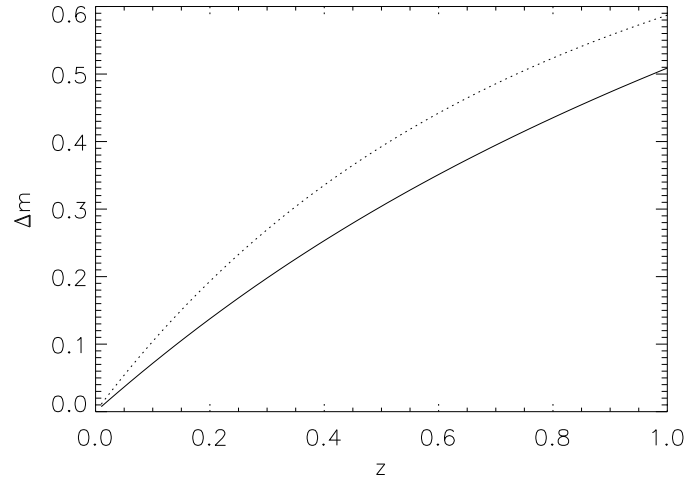


**Figure 6.** The difference in magnitude,  $\Delta m(\Omega_M, \Omega_\Lambda)$ , as a function of redshift for different values of  $\Omega_M$  and  $\Omega_\Lambda$ . The solid line corresponds to  $m(0.3, 0.7) - m(0.3, 0)$  and the dotted line to  $m(0.3, 0.7) - m(1, 0)$ .

that the oscillations exist and lead to a dimming of all SNe. Thus, we need to investigate the axion attenuation as a function of redshift. In figure 6, the difference in observed magnitude for different cosmologies is plotted. If the universe has  $(\Omega_M, \Omega_\Lambda) = (0.3, 0)$

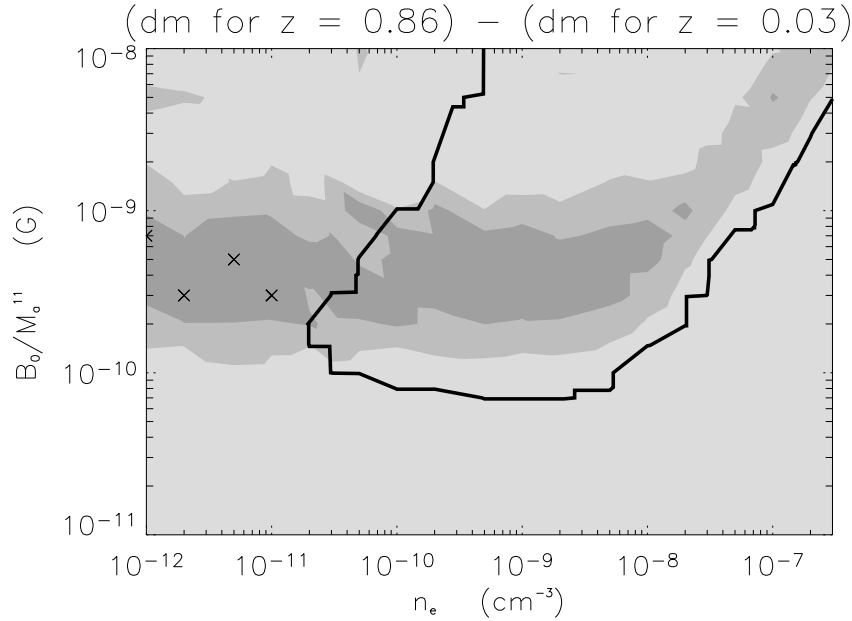


**Figure 7.** The solid line indicates the border to the allowed parameter region. The palest region indicates a difference in attenuation of less than 0.15 magnitudes between a SNIa at  $z = 0.86$  and one at  $z = 0.03$ . The darker region indicates a difference between 0.15 and 0.30 magnitudes and the darkest region a difference larger than 0.30 magnitudes. The ‘x’ indicates allowed simulations with a dimming difference larger than 0.44 magnitudes.

and the observed SN magnitudes is best fitted by a cosmology with  $(\Omega_M, \Omega_\Lambda) = (0.3, 0.7)$ , oscillations need to account for a difference in dimming of 0.44 magnitudes between a SNIa at  $z = 0.86$  and one at  $z = 0.03$ . If instead the universe has  $(\Omega_M, \Omega_\Lambda) = (1, 0)$  we need to be able to explain a dimming of 0.51 magnitudes between  $z = 0.86$  and  $z = 0.03$ . In figure 7, we have plotted the difference in attenuation between  $z = 0.86$  and  $z = 0.03$  for different values of the parameters  $n_e$  and  $B_0/M_a^{11+}$ .

A universe with  $(\Omega_M, \Omega_\Lambda) = (0.3, 0)$ ,  $n_e = 10^{-12} \text{cm}^3$  and  $B_0/M_a^{11+} = 3 \cdot 10^{-10} \text{G}$  where photons mix with axions with a mass  $m_a \lesssim 10^{-16} \text{eV}$  yields almost exactly the same observed magnitudes as a cosmology with  $(\Omega_M, \Omega_\Lambda) = (0.3, 0.7)$  without oscillations (see figure 8). This scenario is not possible to rule out using the observed (lack of) dispersion in quasar spectra. It is also possible to mimic a  $(\Omega_M, \Omega_\Lambda) = (1, 0)$  universe using photon-axion oscillations. However, this requires an uncomfortably low value of the Hubble parameter in order to provide sufficient interaction length. We stress again that since cosmic microwave background observations show that the universe is close to flat and large scale galaxy surveys indicate a low matter density, it is unlikely that all the dimming is caused by photon-axion oscillations. However, the given examples show

<sup>+</sup> Note that the dimming of the simulations are calculated for a universe where  $(\Omega_M, \Omega_\Lambda) = (0.3, 0.7)$ . The effect of the cosmology is, however, small and can be effectively cancelled by small changes in the magnetic field strength and the electron density.

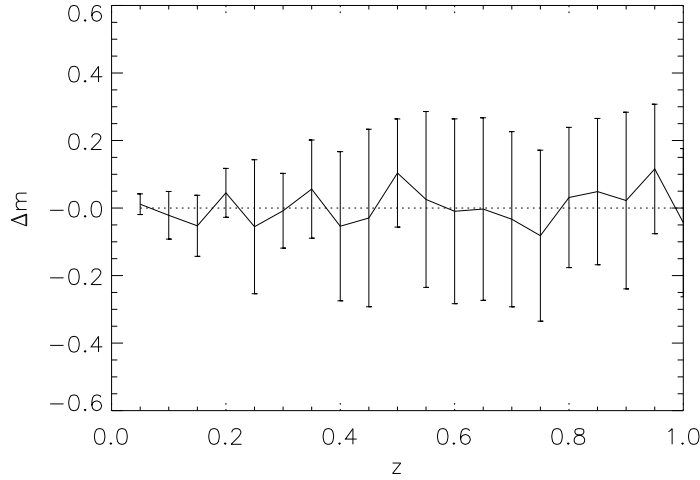


**Figure 8.** The difference in magnitude,  $\Delta m$ , as a function of redshift for  $(\Omega_M, \Omega_\Lambda) = (0.3, 0.7)$  (no oscillations) and an open universe with  $(\Omega_M, \Omega_\Lambda) = (0.3, 0)$  and  $n_e = 10^{-12} \text{cm}^3$  and  $B_0/M_a^{11} = 3 \cdot 10^{-10} \text{G}$ . The error bars correspond to the dispersion induced by inhomogeneities in the magnetic field strength and electron density (see also Section 2.9).

that the systematic effects can be very large and need to be considered when estimating dark energy parameters.

### 2.9. Dispersion in type Ia supernova magnitudes

Since the oscillation probability is independent of photon energy for  $B\omega/(M_a n_e) \gtrsim 9 \cdot 10^{-21} \text{cm}^3 \text{G}$  we cannot use the induced dispersion in quasar spectra to constrain the effect in this region. As an additional constraint, we can instead use the induced dispersion in SNIa magnitudes. If the magnetic field strength and electron density is not perfectly homogeneous, different lines of sight will correspond to different phases in the photon-axion oscillation. This will cause a dispersion also in integrated broad band magnitudes of high redshift sources (see figure 8). Since the dispersion can be of the same order as the attenuation, we should be able to constrain the effect by studying the observed dispersion in SNIa magnitudes.

In figure 9, we plot the B magnitudes of the SNIa in reference [30] as a function of redshift. We construct three redshift bins ( $0 < z < 0.1$ ,  $0.3 < z < 0.7$ , and  $0.7 < z < 1.1$ ) with the mean redshifts 0.03, 0.49, and 0.86, respectively. The magnitude dispersion in the bins are  $0.22 \pm 0.02$ ,  $0.33 \pm 0.04$ , and  $0.30 \pm 0.06$ . We use the first redshift bin to estimate the intrinsic dispersion of the SN magnitudes as  $\sigma_{\text{intr}} = \sqrt{\sigma_{\text{real}}^2 - \sigma_{\text{sim}}^2}$ , where  $\sigma_{\text{real}}$  is the dispersion of the observed SNe and  $\sigma_{\text{sim}}$  is the simulated dispersion caused by photon-axion oscillations at this redshift. We can then correct the simulated dispersions in the higher redshift bins for the intrinsic dispersion and check if the dispersion is larger than observed. For current data, the dispersion is too large to

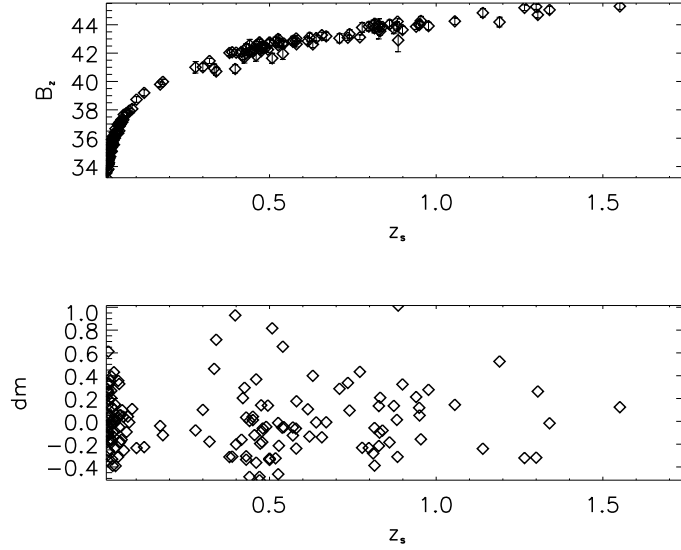


**Figure 9.** The B magnitude and the dispersion in the B magnitude as a function of redshift for some of the SNe in reference [30].

be able to use the effect to give any useful constraints. However, if we would be able to calibrate a future SNIa sample of 50 SNe in each redshift bin,  $z = 0.03, 0.49$  and  $0.86$ , down to an intrinsic dispersion of 0.1 magnitudes, an upper limit of  $\sim 0.3$  magnitudes could be obtained for the difference in attenuation between a SNIa at  $z = 0.86$  and one at  $z = 0.03$ , see figure 10.

### 3. Dust

Dust grains are present both in the interplanetary, interstellar, and intracluster space. It is not known with certainty if there is dust in the intergalactic space. Dust in the Milky Way can be described by a mean extinction law  $A(\lambda) = f(R_V)$  where  $A(\lambda)$  is the extinction for the wavelength  $\lambda$ . Reddening is a consequence of the fact that shorter wavelengths are more effectively absorbed and scattered by dust than longer. It is quantised by the reddening parameter,  $R_V$ , which is defined as

$$R_V \equiv \frac{A_V}{E(B - V)}, \quad (9)$$

where  $A_V$  is the V-band extinction and  $E(B - V)$  is the colour excess,

$$E(B - V) \equiv (B - V)_{\text{obs}} - (B - V)_{\text{intr}}. \quad (10)$$

Here  $(B - V)_{\text{obs}}$  is the observed colour and  $(B - V)_{\text{intr}}$  is the intrinsic colour. Within the Milky Way, we have  $2 \lesssim R_V \lesssim 6$ , but  $R_V \approx 3.1$  is often a useful approximation. Among other galaxies, values of  $R_V$  has been observed in the interval  $1.5 \lesssim R_V \lesssim 7.2$  [34]. Since small particles preferentially scatter light with short wavelengths, a population

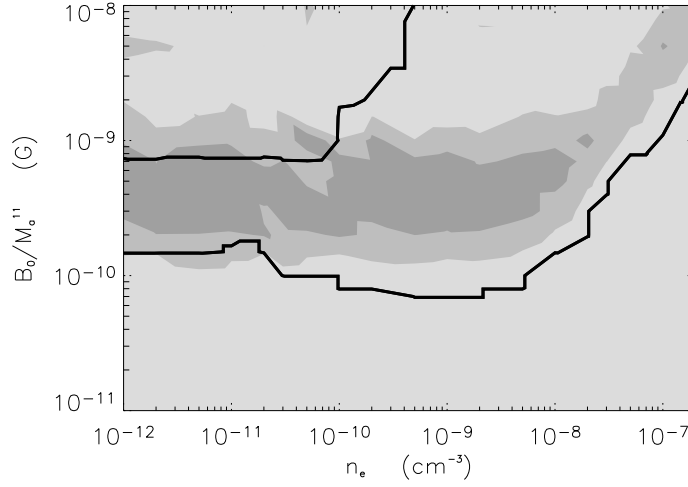


**Figure 10.** The solid line indicates the border to the allowed parameter region combining current quasar constraints and future constraints using the dispersion in SNIa magnitudes. An intrinsic dispersion of 0.1 magnitudes for 50 SNe in each redshift bin  $z = 0.03, 0.49$  and  $0.86$  is assumed. The palest region indicates a difference in attenuation of less than 0.15 magnitudes between a SNIa at  $z = 0.86$  and one at  $z = 0.03$ . The darker region indicates a difference between 0.15 and 0.30 magnitudes and the darkest region a difference larger than 0.30 magnitudes.

of small grains have a lower value of  $R_V$  than a population of large grains. Different parametrisations of  $f(R_V)$  is given in, e.g., Cardelli, Clayton and Mathis (CCM) [31] and Fitzpatrick [32]. In reference [23], the CCM parametrisation was used. In this paper, we compare our results using the different forms of  $f(R_V)$ , finding that the differences are negligible except for very high values of  $R_V$ . Note however that it is not known if any of the parametrisations are valid for an intergalactic dust population with  $R_V \gtrsim 7$ . The results presented in this work are obtained using the  $f(R_V)$  given in Fitzpatrick [32].

### 3.1. Constraining intergalactic dust

The main constraints on the intergalactic dust population are:

- (i) The dust population must not produce such an amount of reddening that it causes discrepancies with observations.
- (ii) The dust must not contribute with more radiation to the background, than what is observed.

The intergalactic dust absorbs energy from the optical and the UV background and then emits it in the far-infrared. This can be used to constrain the intergalactic dust since it cannot contribute with more radiation in this wavelength region than what has not been identified as other sources. A universe where the dimming of SNIa is explained solely

by intergalactic dust probably cannot have  $(\Omega_M, \Omega_\Lambda) = (1, 0)$ , while  $(\Omega_M, \Omega_\Lambda) = (0.2, 0)$  cannot be ruled out [33].

In this paper we will use the reddening of high redshift sources to constrain the properties of intergalactic dust and the effects on SN observations (see also reference [35]). This is accomplished with colour comparisons of real quasars with simulated quasars for different dust scenarios.

### 3.2. Theory of the simulations

We assume a quasar (or a SN) at a certain redshift and follow the photons emitted from the source to the detector at Earth using SNOOC [27]. The path of the photons is divided into cells of the same size as the average distance between galaxies. In each cell, the dust density and the differential extinction coefficient is specified and the extinction due to intergalactic dust is calculated.

The dust attenuation,  $\Delta m_{\text{dust}}$ , at a given emission redshift  $z_e$  and a given observed wavelength is given by  $\lambda_o$  [23]

$$\Delta m_{\text{dust}}(z_e, \lambda_o) = \frac{2.5}{\ln 10} \int_0^{z_e} \frac{A(\lambda_o/(1+z), R_V)/A(V)}{D_V(z)H(z)(1+z)} dz, \quad (11)$$

where  $A(V)$  is the attenuation in the V-band and  $D_V$  is the interaction length for photon scattering or absorption with dust particles in the V-band. The function  $H(z)$  is given by

$$H(z) = H_0 \sqrt{(1+z)^3 \Omega_M + (1+z)^2 (1 - \Omega_M - \Omega_\Lambda) + \Omega_\Lambda}. \quad (12)$$

We study two different models of the dust distribution with  $\rho_{\text{dust}} \propto (1+z)^{\alpha(z)}$  and  $\alpha(z)$  given by [27, 23]:

Model A:  $\alpha(z) = 3 \forall z$

$$\text{Model B: } \alpha(z) = \begin{cases} 3 & \forall z \leq 0.5 \\ 0 & \forall z > 0.5 \end{cases}$$

Model A corresponds to a dust population with a constant comoving density whereas model B corresponds to a population where dust is created at redshifts  $z > 0.5$  with the same rate as the dilution caused by the expanding universe. The two models represent two extremes in a scale of dust models and they can therefore be considered to capture a wide range of possible dust models.

Since  $D_V(z) = [\sigma n_{\text{dust}}(z)]^{-1}$ , where  $\sigma$  is the interaction cross section and  $n_{\text{dust}}(z)$  is the dust number density, we have  $D_V(z) \propto \rho_{\text{dust}}^{-1} \propto (1+z)^{-\alpha(z)}$ . The proportionality constant is determined by  $D_{0V}$ , the interaction length for the V-band at zero redshift.

### 3.3. Observed quasar colours

We use the same sample of 16 713 quasars from the SDSS DR1 [28] described in Section 2.4. The 821 quasars that have been classified as extended are excluded to avoid problems with contamination from the host galaxy.

To avoid quasars with too much noise, we only include objects with magnitudes brighter than 22.3, 22.6, 22.7, 22.4, and 20.5, respectively for the five filters (u, g, r, i, and z), corresponding to a signal-to-noise (S/N) ratio better than 5:1 [36]. This leaves 15 194 quasars.

We also restrict ourselves to redshifts  $0.5 < z < 2$ . This is primarily because we want to have good statistics, i.e., many quasars in every redshift bin. Another reason for excluding objects with redshifts  $z < 0.5$  is that quasar spectra at these redshifts often are contaminated by their host galaxy. Finally we have 11 694 point-like quasars with redshifts  $0.5 < z < 2$  that fulfill the S/N limit.

The quasars are divided into redshift bins of size  $\Delta z = 0.05$ . For each bin, the mean colour,  $(X - Y)_z^{\text{obs}}$ , is calculated for all combinations of different filters, X and Y. Objects with a colour more than two standard deviations from the mean value is rejected. This is because we are not interested in using peculiar quasars that have evolved under unusual circumstances.

### 3.4. Simulated quasar colours

We assume a universe with  $[\Omega_M = 0.3, \Omega_\Lambda = 0.7, h = 0.7]$  and simulate dust scenarios with  $10 \text{ Gpc} \leq D_{0V} \leq 5000 \text{ Gpc}$  and  $0 \leq R_V \leq 12$ . Each parameter set  $(R_V, D_{0V})$  is simulated twice, once for each dust model described in Section 3.2. For each scenario, a large number of quasar events are simulated with different values of the redshift. For each event, the K correction for the SDSS broadband filters u, g, r, i, and z is generated using the median quasar spectrum obtained in reference [29]. The simulated mean colour,  $(X - Y)_{z, R_V, D_{0V}}^{\text{sim}}$ , is calculated by subtracting the K corrections for the filters, which is the same as subtracting the two filter magnitudes.

The probability of the different scenarios are determined with the  $\chi^2$ -function

$$\chi^2 = \sum_{i,j=1}^N \Delta(X - Y)_{z_i, R_V, D_{0V}} (V(X - Y)^{-1})_{i,j} \Delta(X - Y)_{z_j, R_V, D_{0V}}, \quad (13)$$

$$\Delta(X - Y)_{z, R_V, D_{0V}} = (X - Y)_z^{\text{obs}} - (X - Y)_{z, R_V, D_{0V}}^{\text{sim}}, \quad (14)$$

where  $i$  and  $j$  refer to the redshift bins. The covariance matrix  $V(X - Y)_{i,j}$  is defined as

$$V(X - Y)_{i,j} = \sigma(X)_{\text{sys}}^2 + \sigma(Y)_{\text{sys}}^2 + \delta_{ij} [\sigma(X)_{\text{tem}}^2 + \sigma(Y)_{\text{tem}}^2 + \sigma(X - Y)_{\text{obs}}^2], \quad (15)$$

where  $\sigma_{\text{sys}}(i)$  is the systematic error and  $\sigma_{\text{tem}}(i)$  is the template error associated with the broadband filter  $i$ . The template errors arise because we use a median quasar spectrum in the simulation of the K corrections and not all rest frame quasar spectra are identical. The systematic filter errors are 0.03 for the u and z filters and 0.02 for the others, while the template errors have been estimated to 0.1 for the u and z filter and to 0.05 for the other filters.  $\sigma_{\text{obs}}$  denotes the deviation from the mean observed colour in each redshift bin. Note that the error budget is completely dominated by the template error. The inclusion of quasar data from the second and third data release of the SDSS will therefore have a small effect on the constraints obtained.

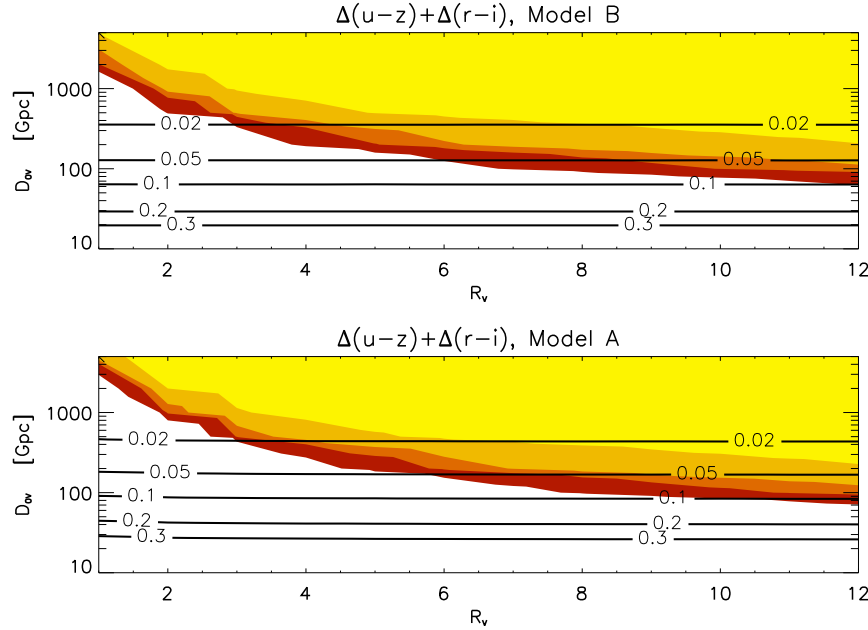


**Figure 11.** The confidence levels combining  $\Delta(u-z)$  and  $\Delta(r-i)$  for the two dust models and the attenuation of a SNIa at  $z = 1$ . The palest region indicates the 68% confidence level allowed by the  $\chi^2$ -test and the darker regions indicate 90%, 95%, and 99%. The almost horizontal lines show the B-band attenuation in magnitudes caused by dust for a SNIa at  $z = 1$ .

### 3.5. Result

In figure 11, we present our results from the  $\chi^2$ -analysis combining  $\Delta(u-z)$  and  $\Delta(r-i)$  together with the expected dimming in the B-band,  $\Delta m_B(z)$ , for a SNIa at the  $z = 1$ . We conclude that at 99% confidence level, the dimming in the B-band  $\Delta m_B \lesssim 0.1$  for a SNIa at  $z = 1$ . We can also limit the interaction length for the V-band at  $z = 0$  to be larger than 60 Gpc. If the intergalactic dust is similar to the Milky Way dust (with  $R_V \lesssim 4$ ), we are able to rule out  $\Delta m_B \gtrsim 0.03$ .

If we use the CCM parametrisation instead of the parametrisation by Fitzpatrick we get an upper limit on the B-band dimming of a SNIa at  $z = 1$  of 0.2 magnitudes.

Note that the scenario without any intergalactic dust is not eliminated by the analysis. Also, the increase in the number of quasars and the improvement of the systematic filter errors of the SDSS DR1 compared to the EDR have led only to minor improvements compared to the results obtained in reference [23].

## 4. Summary

Observations of high redshift SNIa show that the universe is dominated by dark energy accelerating the expansion rate. In order to take advantage of the increased SN statistics and to be able to use SNIa data to determine the dark energy properties, it is necessary



to control the systematic effects involved. We have used quasar colours and spectra from the SDSS DR1 to constrain the effects from intergalactic dust attenuation and photon-axion oscillations, respectively.

We have found that the largest possible dimming of a SNIa at  $z = 1$  caused by intergalactic dust is 0.2 magnitudes. The addition of new quasars to the intergalactic dust analysis will not improve the limits since the analysis is limited by systematic errors, in particular the template errors. One way of improving the template errors is to use different template spectra for different groups of quasars. For example, a median spectrum created from low redshift quasars will be unaffected by possible intergalactic dust and photon-axion oscillations. If the template errors were half their size, we would be able to give a maximum dimming limit of 0.05 magnitudes for a SNIa at  $z = 1$ . Also, improving the resolution of the FIRB experiments could lead to the rejection of more dust scenarios. The calculations of the dimming caused by intergalactic dust is based on mean extinction laws for the dust in the Milky Way [31, 32]. It is not known if these parametrisations are valid for an intergalactic dust population where  $R_V$  might be much larger than in the interstellar medium. Also, we have assumed that the reddening parameter,  $R_V$ , is independent of direction and redshift. However, this is an excellent approximation since the simulated SN attenuation is almost independent of  $R_V$  (see e.g. figure 11).

For photon-axion oscillations we have found a maximum dimming of 0.1 magnitudes for SNIa at  $z = 1$  if  $B\omega/(M_a n_e) \lesssim 9 \cdot 10^{-21} \text{ cm}^3\text{G}$ , where  $B$  is the magnetic field strength,  $\omega$  is the photon energy,  $M_a$  is the inverse coupling between the photon and the axion, and  $n_e$  is the electron density. However, when  $B\omega/(M_a n_e) \gtrsim 9 \cdot 10^{-21} \text{ cm}^3\text{G}$ , the oscillation probability is independent of photon energy and a dimming as large as 0.6 magnitudes cannot be excluded. We have also shown that for certain values of  $n_e$  and  $B/M_a^{11}$ , the attenuation from oscillations evolve with redshift in a manner very similar to the observed SNIa dimming.

The region where the effect is independent of photon energy could be constrained using the observed dispersion in SNIa magnitudes. An inhomogeneous magnetic field strength and/or electron density will cause different lines of sight to correspond to different phases in the photon-axion oscillation. Thus we expect a dispersion in integrated broad band magnitudes of high redshift sources if oscillations are present. We have shown that it is not possible to use current data to obtain any further constraints on this region. However, a future SNIa sample of 50 SNe in each redshift bin  $z = 0.03, 0.49$  and  $0.86$  with an intrinsic dispersion of 0.1 mag, would yield an upper limit of  $\sim 0.3$  magnitudes difference in attenuation between a SNIa at  $z = 0.86$  and one at  $z = 0.03$ .

## Acknowledgments

The authors would like to thank Ariel Goobar and Lars Bergström for useful discussions and Ching Wa-Yip for valuable help with the SDSS Data Archive Server.

Funding for the creation and distribution of the SDSS Archive has been provided by

the Alfred P. Sloan Foundation, the Participating Institutions, the National Aeronautics and Space Administration, the National Science Foundation, the US Department of Energy, the Japanese Monbukagakusho, and the Max Planck Society. The SDSS Web site is <http://www.sdss.org/>. The Participating Institutions are the University of Chicago, Fermilab, the Institute for Advanced Study, the Japan Participation Group, the Johns Hopkins University, the Max Planck Institute for Astronomy (MPIA), the Max Planck Institute for Astrophysics (MPA), New Mexico State University, Princeton University, the United States Naval Observatory, and the University of Washington.

## References

- [1] Bennett C L et al 2003 *Astrophys. J. Suppl.* **148** 1  
(Bennett C L et al 2003 *Preprint* arXiv:astro-ph/0302207)
- [2] Spergel D N et al 2003 *Astrophys. J. Suppl.* **148** 175  
(Spergel D N et al 2003 *Preprint* astro-ph/0302209)
- [3] Colless M et al 2003 *Preprint* arXiv:astro-ph/0306581
- [4] Tegmark M et al [SDSS Collaboration] 2003 *Preprint* arXiv:astro-ph/0310723
- [5] Tegmark M et al [SDSS Collaboration] 2003 *Preprint* arXiv:astro-ph/0310725
- [6] Domínguez I et al 1998 *Preprint* astro-ph/9809292
- [7] Riess A G et al 1998 *Astron. J.* **116** 1009-1038  
(Riess A G et al 1998 *Preprint* astro-ph/9805201)
- [8] Perlmutter S et al 1999 *Astrophys. J.* **517** 565-586  
(Perlmutter S et al 1998 *Preprint* astro-ph/9812133)
- [9] Sullivan M et al 2003 *Mon. Not. Roy. Astron. Soc.* **340** 1057  
(Sullivan M et al 2002 *Preprint* astro-ph/0211444)
- [10] Höflich P, Wheeler J C and Thielemann F K 1998 *Astrophys. J.* **495** 617  
(Höflich P, Wheeler J C and Thielemann F K 1997 *Preprint* astro-ph/9709233)
- [11] Riess A G et al 1999 *Astron. J.* **118** 2668  
(Riess A G et al 1999 *Preprint* astro-ph/9907038)
- [12] Amanullah R, Mörtzell E and Goobar A 2003 *Astron. Astrophys.* **397** 819-823  
(Amanullah R, Mörtzell E and Goobar A 2002 *Preprint* astro-ph/0204280)
- [13] Kolb E W, Matarrese S, Notari A, Riotto A 2004 *Preprint* hep-ph/0409038
- [14] Räsänen S 2004 *JCAP* **0402** 003
- [15] Csáki C, Kaloper N and Terning J 2002 *Phys. Rev. Lett.* **88** 161302  
(Csáki C, Kaloper N and Terning J 2001 *Preprint* hep-ph/0111311)
- [16] Deffayet C, Harari D, Uzan J-P and Zaldarriaga M 2002 *Phys. Rev.* **D66** 043517  
(Deffayet C, Harari D, Uzan J-P and Zaldarriaga M 2001 *Preprint* hep-ph/0112118)
- [17] Csáki C, Kaloper N and Terning J 2002 *Phys. Lett.* **B535** 33-36  
(Csáki C, Kaloper N and Terning J 2001 *Preprint* hep-ph/0112212)
- [18] Mörtzell E, Bergström L and Goobar A 2002 *Phys. Rev.* **D66** 047702  
(Mörtzell E, Bergström L and Goobar A 2002 *Preprint* astro-ph/0202153)
- [19] Christensson M and Fairbairn M 2003 *Phys. Lett.* **B565** 10-18  
(Christensson M and Fairbairn M 2002 *Preprint* astro-ph/0207525)
- [20] Csáki C, Kaloper N, Terning J 2004 *Preprint* astro-ph/0409596
- [21] Aguirre A N 1999 *Astrophys. J.* **512** L19  
(Aguirre A N 1998 *Preprint* astro-ph/9811316)
- [22] Aguirre A N 1999 *Astrophys. J.* **525** 583  
(Aguirre A N 1999 *Preprint* astro-ph/9904319)

- [23] Mörtzell E and Goobar A 2003 *JCAP* **0309** 009  
(Mörtzell E and Goobar A 2003 *Preprint* astro-ph/0308046)
- [24] Mörtzell E and Goobar A 2003 *JCAP* **0304** 003  
(Mörtzell E and Goobar A 2003 *Preprint* astro-ph/0303081)
- [25] Raffelt G G 1996 *Stars as Laboratories for Fundamental Physics: The Astrophysics of Neutrinos, Axions, and Other Weakly Interacting Particles* (Chicago: University Press)
- [26] Sakurai J J 1995 *Modern Quantum Mechanics* (Reading: Addison-Wesley Publishing Company)
- [27] Goobar A et al 2002 *Astron. Astrophys.* **392** 757-771  
(Goobar A et al 2002 *Preprint* astro-ph/0206409)
- [28] Schneider D P et al 2003 *Astron. J.* **126** 2579  
(Schneider D P et al 2003 *Preprint* astro-ph/0308443)
- [29] Vanden Berk D E et al 2001 *Astron. J.* **122** 549-564  
(Vanden Berk D E et al 2001 *Preprint* astro-ph/0105231)
- [30] Riess A G et al [Supernova Search Team] 2004 *Astrophys. J.* **607** 665  
(Riess A G et al [Supernova Search Team] 2004 *Preprint* astro-ph/0402512)
- [31] Cardelli J A, Clayton G C and Mathis J S 1989 *Astrophys. J.* **345** 245-256
- [32] Fitzpatrick, E. L. 1999 *PASP* **111** 63-75
- [33] Aguirre A and Haiman Z 2000 *Astrophys. J.* **532** 28  
(Aguirre A and Haiman Z 2000 *Preprint* astro-ph/9907039).
- [34] Falco E E et al 1999 *Preprint* astro-ph/9901037
- [35] Goobar A, Bergström L and Mörtzell E 2002 *Astron. Astrophys.* **384** 1
- [36] Richards G T et al [SDSS] 2001 *Astron. J.* **121** 2308  
(Richards G T et al [SDSS] 2000 *Preprint* astro-ph/0012449)